Direct Observation of Bicarbonate and Water Reduction on Gold: Understanding the Potential Dependent Proton Source During Hydrogen Evolution

Gang-Hua Deng[1], Quansong Zhu[2], Jaclyn Rebstock[2], Tomaz Neves-Garcia[2], L. Robert Baker[2*]

[1] State Key Laboratory of Information Photonic and Optical Communications and School of Science, Beijing University of Posts and Telecommunications (BUPT), Beijing 100876, P. R. China

[2] Department of Chemistry and Biochemistry, The Ohio State University, Columbus, Ohio 43210, United States

[*] E-mail: baker.2364@osu.edu
Phone: +1 (614) - 292 - 2088

1. Experimental

The details of the SFG system have been described previously[1-4]. Briefly, a Ti: sapphire regenerative amplifier (Spectra Physics-Solstice) with a pulse duration of ~90 fs pulses (2 kHz, 7 W) at 800 nm is used at the pump laser. 70% of the output is used to pump an optical parametric amplifier (TOPAS Prime), which directs the signal and idler to a noncollinear difference frequency generation (DFG) stage. The rest 30% is spectrally narrowed to ~10 cm^{-1} using an air-gap etalon (TecOptics). The beams are incident on the sample at 56° in a Kretschmann configuration. The IR beam is centered at ~3450 cm^{-1} in the OH stretch region with an energy of 3 μJ. The energy of the picosecond 800 nm is around 10 μJ. In measurements of the water spectra, a potential step ranging from −0.1 to −1.2 V vs Ag/AgCl was applied to the Au electrode, and each spectrum was collected by delaying the visible beam relative to the IR beam by ~500 fs, with an integration time of 2 min. The details of the VSFG electrochemical cell can be found in our previous studies.[1, 2, 4] The VSFG electrochemical cell adopted a backside geometry with plasmon enhancement. Such VSFG electrochemical cell enables us to do in situ measurements of the Au/electrolyte interface at current densities exceeding 1 mA/cm^2 in the absence of mass transport limitations.[1, 2]

Two types of polycrystalline Au were used in the measurements. The Au electrodes for SFG measurements were manufactured by depositing 35 nm of Au onto CaF_2 windows through electron beam evaporation (Denton DV-502A E-Gun Evaporator). Before Au deposition, the CaF_2 windows were cleaned with basic Piranha solution (5:1:1 $H_2O/H_2O_2/NH_4OH$) at 80 °C for 1 h. The other type of Au electrodes (denoted as Cr/Au), which were used for electrochemical measurements and FE measurements, were produced with the same equipment. The difference was that a 20 nm chromium adhesion layer was deposited onto the glass substrates before a 100 nm layer of Au was deposited on the top. Before each experiment, the Cr/Au was cleaned by sonication in ethanol for 5 min first, followed by sonication in copious amounts of Milli-Q water three times.

Electrochemical measurements were carried with a BioLogic SP-50 potentiostat. The electrochemical cell consisted of a Au working electrode, a leakless Ag/AgCl reference electrode

(eDAQ ET072-1), and a Pt mesh counter electrode. The cathode and anode compartments were separated by a Nafion membrane. The electrolytes were prepared by purging 0.05 M Na_2SO_4 (99.99%) with Ar or CO_2 (Praxair, 99.999%) for 20 min.

The procedure of determining the Faradaic efficiencies for CO and H_2 has been described in our previous work[4, 5]. Briefly, an Agilent 7890B gas chromatograph was connected to the electrochemical H-cell through a custom headspace sampling system. The H-cell has two compartments separated by a Nafion membrane. The Nafion membrane was activated in 10% H_2SO_4 at 80°C for 10 min before each measurement. A Pt film was used as the counter electrode, and a Ag/AgCl electrode was used as the reference electrode. The electrolyte used in the measurements are 0.05 M Na_2SO_4 and 0.1 M $NaHCO_3$ (99.997%). Before the measurement, the electrolyte was purged with Ar or CO_2 for 20 min at a rate of 0.35 L/min, and the headspace of the H-cell was filled with Ar or CO_2. During the measurement, a constant potential of −1.2 V vs Ag/AgCl was applied to the Cr/Au working electrode for 30 min by a Biologic SP-50 potentiostat, after which a gas sample from the headspace was injected into the GC.

2. Isotope exchange experiments and non-equilibrium nature of OH^-

To further confirm the assignment of the peak around 3650 cm^{-1}, a control experiment was carried out by using isotope exchange. The potential was held at -1.1V and the electrochemical cell was flushed with D_2O electrolyte (0.05M Na_2SO_4 solution), the peak disappeared gradually in 6 minutes as shown in Figure S1. The red curve is measured with 0.05M Na_2SO_4 solution in H_2O. Both the peaks of surface OH^- (3650 cm^{-1}) and free OH (3730 cm^{-1}) of surface water molecules are very prominent. Once the cell was flushed with D_2O electrolyte, the peak intensity of surface OH^- dropped significantly and disappeared completely at 8 minutes.

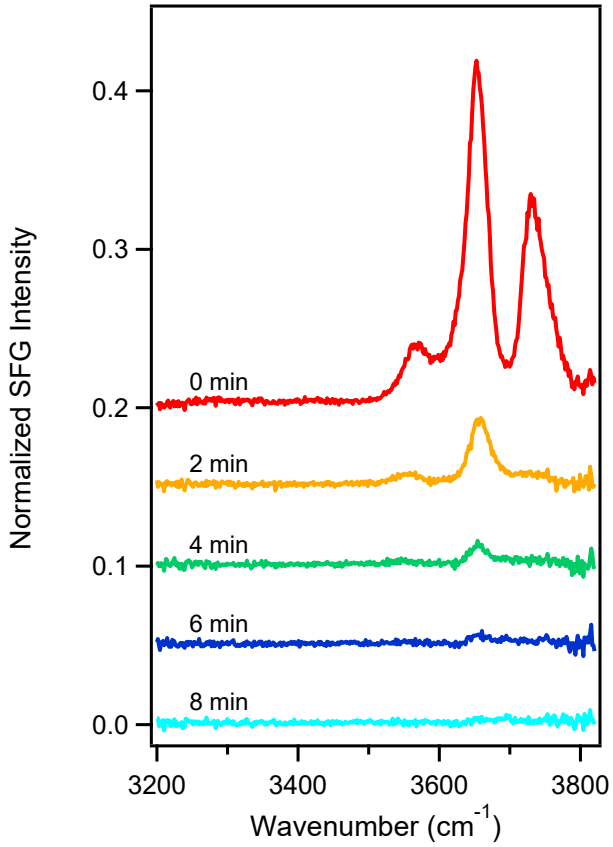

Figure S1. SFG spectra at OH stretch region for Na_2SO_4 (0.05 M) purged with Ar at -1.1V vs Ag/AgCl. Initially, the solution was in H_2O, as the cell flushing with D_2O electrolyte, both the OH^- peak around 3650 cm^{-1} and free OH around 3730 cm^{-1} disappeared.

Once the cell is filled with D_2O electrolyte, the signal at the OH stretch region completely disappeared. Meanwhile, in the OD stretch region, similar to the OH stretch region, two sharp peaks around 2690 cm^{-1} and 2741 cm^{-1} appeared (Figure S2), corresponding to the peak in the OH stretch region around 3650 cm^{-1} and 3730 cm^{-1} respectively. The peak at 2690 cm^{-1} can be assigned to surface OD^- and 2741 cm^{-1} can be assigned to free OD of surface water molecules.[6-9] This further proves that the sharp peaks in the OH stretch region are not because of contamination or artifact.

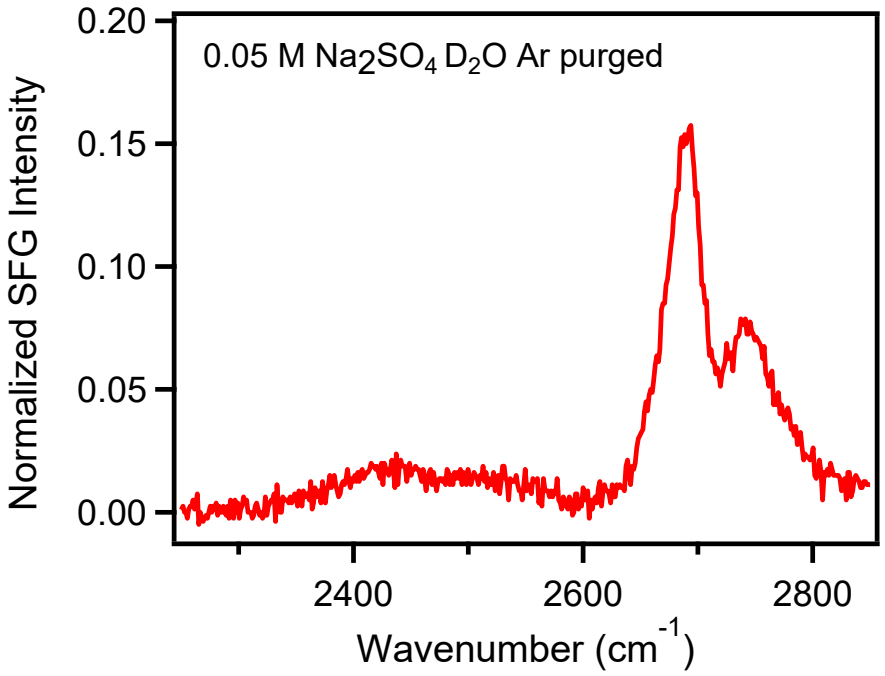

Figure S2. SFG spectra at OD stretch region for Na_2SO_4 (0.05 M D_2O) purged with Ar at -1.1V vs Ag/AgCl.

If the peak around 3650 cm^{-1} under catalytic potentials is due to non-equilibrium OH^-, then when the potential was step above the onset of HER, the peak should disappear. Indeed, as shown in Figure S4, the potential was first set to -1.1V at which potential OH^- is constantly generated at the electrode surface, the peak around 3650 cm^{-1} showed up in the spectrum (red curve) for Ar-saturated 0.05M Na_2SO_4 solution. When the potential was stepped to -0.5V which is above the onset potential of HER, the peak around 3650 cm^{-1} disappeared.

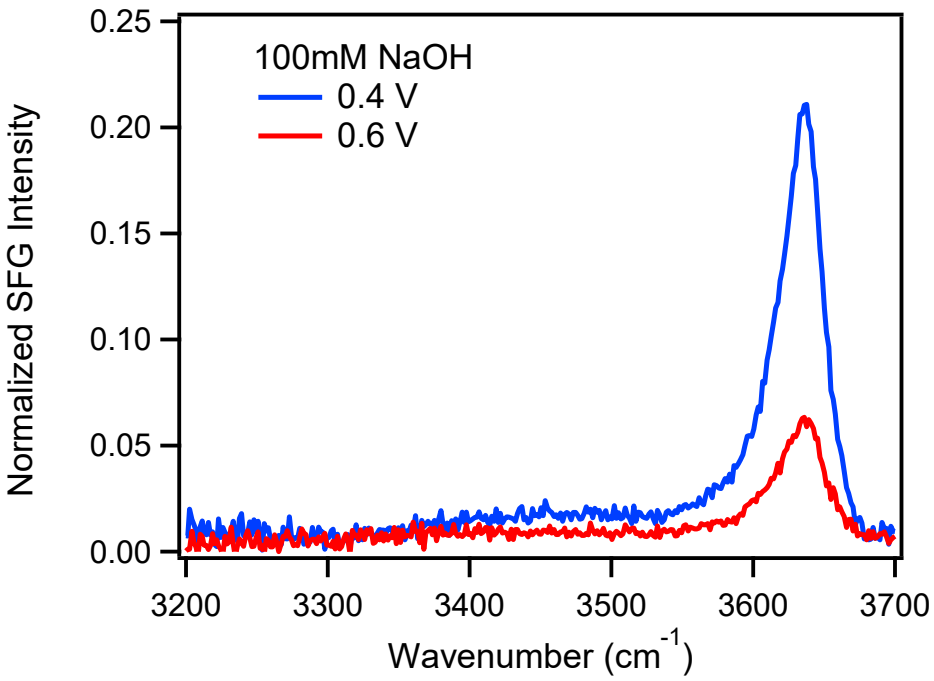

Figure S3. Normalized VSFG spectra of 100 mM NaOH solution at 0.4 and 0.6 V Vs Ag/AgCl

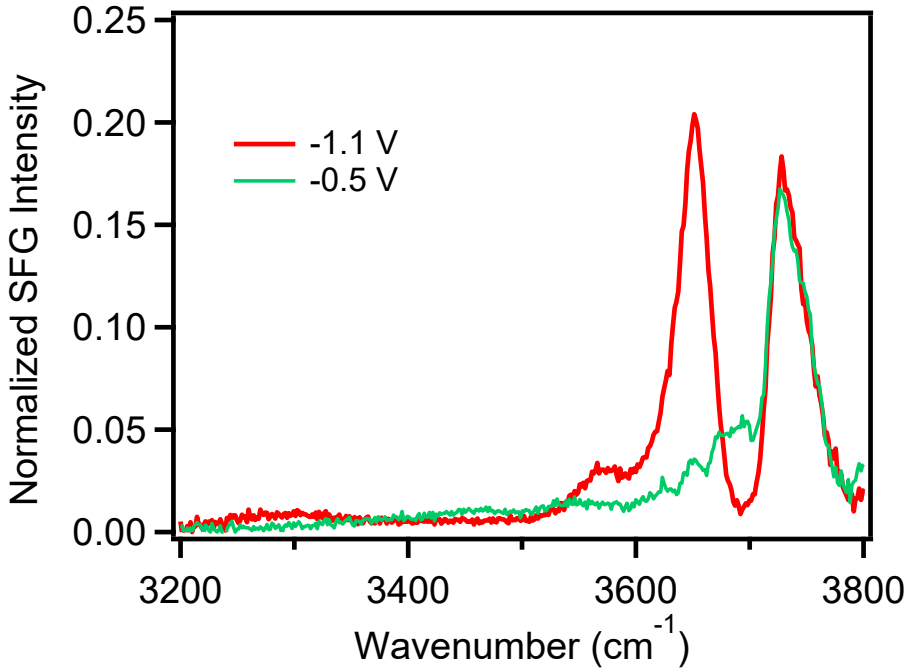

Figure S4. SFG spectra at OH stretch region for Na_2SO_4 (0.05 M) purged with Ar at different potential vs Ag/AgCl. The potential was initially held at -1.1 V (red) and then was switched to -0.5 V (green).

3. Effects of various electrolyte compositions on the interfacial water spectrum

To confirm the origin of the peak around 3400 cm^{-1}, interfacial water spectra of various electrolyte compositions were measured and shown in Figure S5. All spectra were measured at a fixed potential of -1.0V. Figure S5 shows that this peak is weak in Ar-purged NaCl (blue curve). And becomes much more prominent in CO_2-purged NaCl as well as Ar- or CO_2-purged $NaHCO_3$ electrolytes. This confirms that there is a close correlation between this feature and the presence of carbonate species at the interface. The peak intensity around 3400 cm^{-1} mostly contributes from carbonate species.

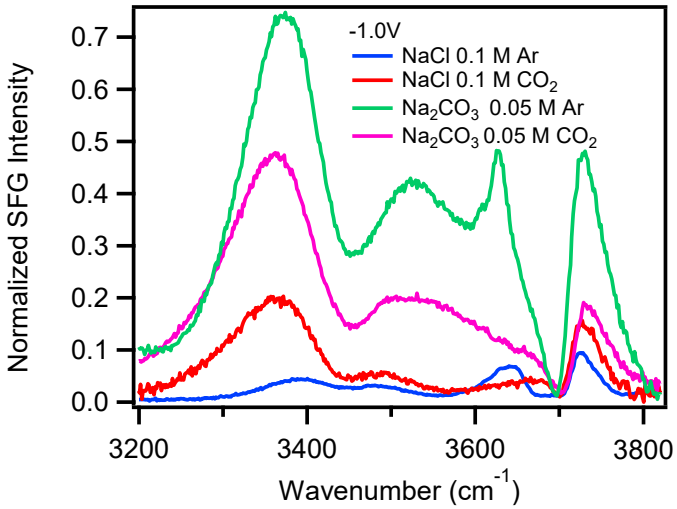

Figure S5 SFG spectra at OH stretch region for NaCl (0.1 M) purged with Ar (blue) or CO_2 (red) and for Na_2CO_3 (0.1 M) purged with Ar (green) or CO_2 (purple) at a potential of -1.0 V vs Ag/AgCl.

4. Concentration dependent spectra of CO_2-saturated Na_2CO_3 solutions

Additionally, we show that at a fixed potential the intensity of this feature tracks closely with the $NaHCO_3$ electrolyte concentration. If the 3400 cm^{-1} is mainly induced by Na^+ and CO_3^{2-} ion pairing then with high concentrations the peak should be more intense because ion pairing is more severe with high concentrations. Figure S6 shows the concentration dependent spectra of the CO_2-saturated Na_2CO_3 solution. It can be seen that with higher concentration of electrolyte, the peak around 3400 cm^{-1} gets more predominant in the spectra which further supports the assignment of the 3400 cm^{-1} peak.

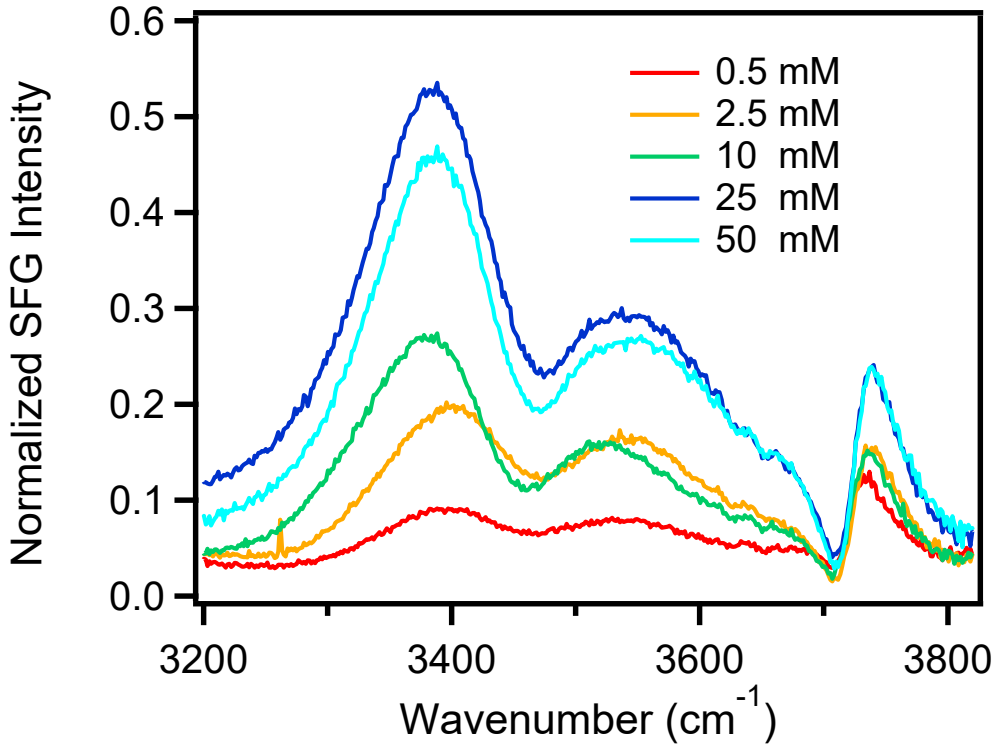

Figure S6. SFG spectra at OH stretch region for CO_2-saturated Na_2CO_3 solutions with different concentrations (0.5, 2.5, 10, 25, 50 mM) at -0.9 V vs Ag/AgCl.

5. Relative concentrations of H_2CO_3, HCO_3^- and CO_3^{2-} as a function of pH

The relative concentrations of $H_2CO_3/CO_2(eq)$, HCO_3^-, and CO_3^{2-} are determined by the pH of the solution. Figure S7 shows the relative concentrations of H_2CO_3, HCO_3^-, and CO_3^{2-} as a function of pH. The calculation of the relative concentrations are based on the dynamic equilibrium between carbon dioxide, carbonic acid, bicarbonate, and carbonate[10-12]. Carbonic acid is the dominant species at pH values below the pK_1 (~6.3), bicarbonate dominates between the pK_1 and pK_2 (~10.3) values and the carbonate ion dominates at pH values above the pK_2. K_1 and K_2 are the first and second dissociation constants of carbonic acid respectively.

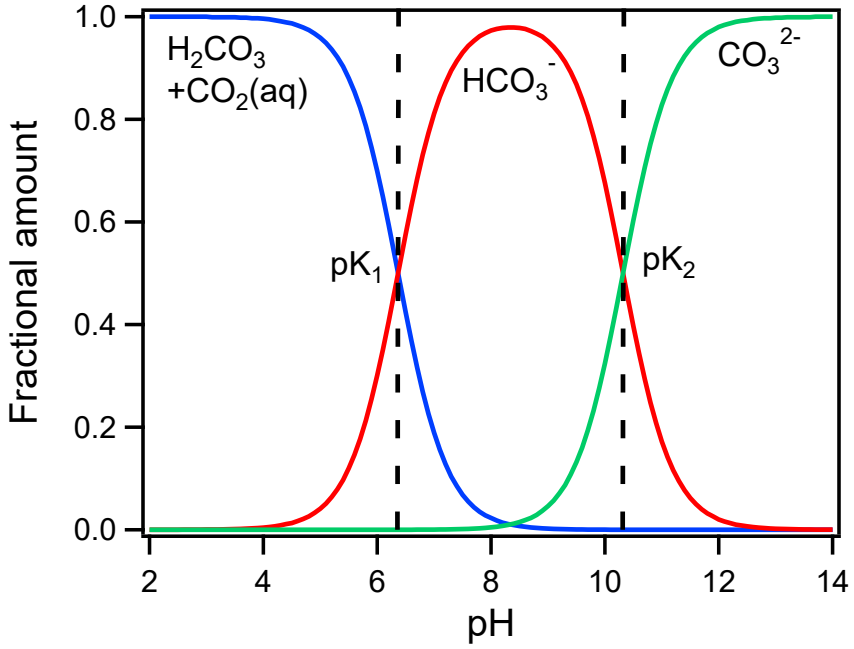

Figure S7. Mole fractions of $H_2CO_3/CO_2(eq)$, HCO_3^-, and CO_3^{2-} as a function of the pH of the dissolved solution.

6. $\chi^{(3)}$ bulk contribution

Disentangling the $\chi^{(3)}$ bulk contribution is critical to gain a detailed physical picture of the Stern layer. Despite the importance of $\chi^{(3)}$ for quantitative analysis of the interfacial water structure, we find that $\chi^{(3)}$ bulk contribution has a minimal influence on the shape of the measured spectra reported here for the reasons described below:

First, in these experiments, in order to suppress the non-resonant signal from the gold electrode, the picosecond 800 nm pulse was delayed by 467 fs with respect to the femtosecond IR pulse. With such a delay, not only the non-resonant signal from the gold electrode is suppressed, but the $\chi^{(3)}$ bulk contribution is also suppressed. For charged surface, the SFG signal is given by:[8, 13-16] $\chi_{eff}^{(2)} = \chi_s^{(2)} + \chi_B^{(3)}\Phi$, in which $\chi_{eff}^{(2)}$ is the total SFG response. $\chi_s^{(2)}$ is the surface contribution. $\chi_B^{(3)}$ is the bulk contribution induced by the interfacial electric field and Φ is the surface potential. There is a consensus in the SFG community that the surface contribution $\chi_s^{(2)}$ comes from only a few topmost monolayers of water molecules. On the contrary, the region contributing to the $\chi_B^{(3)}$ bulk signal can extend into the liquid phase as far as the electric field penetrates. This region is also called the diffuse layer which has an effective thickness defined by the Debye length. Water in this region behaves like bulk water. The vibrational lifetime of the OH stretch of bulk water is ~200 fs [17] which is much shorter than the delay time (467 fs) between IR and picosecond 800 nm pulse. For exponential decay, $e^{-467/200}$=0.097, which indicates at a delay time of 467 fs, less than 10% of the vibrational signal of bulk water was detected in our experiments. Thus most of the $\chi_B^{(3)}$ bulk signal was suppressed. On the other hand, based on a previous study by Borguet and co-workers[18] the vibrational lifetime of hydrogen-bonded OH stretch of interfacial water (which contributes to the $\chi_s^{(2)}$,) at electrolyte/silica interface, is ~ **700 fs** for electrolyte concentration larger than 0.01 M. For a delay time of 467 fs, $e^{-467/700}$=0.513, which indicates that more than 50% of the vibrational signal of interfacial water was detected in our experiments. The vibrational lifetime of hydrogen-bonded OH stretch of interfacial water (700 fs) is substantially longer than that of bulk water (200 fs), thus the delay time of 467 fs for IR and 800 nm pulses gives us a good chance to suppress the $\chi_B^{(3)}$ bulk signal and get the interfacial water $\chi_s^{(2)}$ signal at the same time. The vibrational lifetime of the free OH of the first layer water and surface OH^- generated by water reduction should be substantially longer than hydrogen-bonded interfacial water molecules, and a previous work by Xiao et al [19] showed that the vibrational lifetime of free OH at hydrophobic surface is 1.3 ps. Since the gold surface is also hydrophobic, we have good reason to believe that the vibrational lifetime of free OH at the gold surface should be around ~1.3ps. Such a long vibrational lifetime enables us to detect the free OH signal at a 467 fs delay time of IR and 800 nm. We can estimate the $\chi_B^{(3)}$ contribution based on the vibrational lifetime. As shown in a previous study by Montenegro et al [8], at the water/graphene electrode interface, the $\chi_B^{(3)}$ contribution is slightly smaller than the $\chi_s^{(2)}$. Both the $\chi_s^{(2)}$ and $\chi_B^{(3)}$ are a function of applied potential. $\chi_B^{(3)}$ follows linear response but $\chi_s^{(2)}$ response is not linear. For simplicity, we assume the $\chi_s^{(2)}$ surface signal remains the same as the potential changes. Given the vibrational lifetime of bulk water (200 fs) and interfacial water (700 fs), the $\chi_B^{(3)}$ contribution is estimated

for 467 fs delay time of IR and 800 nm and is shown in the following Figure S8. Apparently, the $\chi_B^{(3)}$ contribution is less than 20% across the potential range. As shown in the previous study by Montenegro et al [8], $\chi_s^{(2)}$ also increases for larger potential, so the estimated $\chi_B^{(3)}$ contribution should be even smaller than shown in Figure S8.

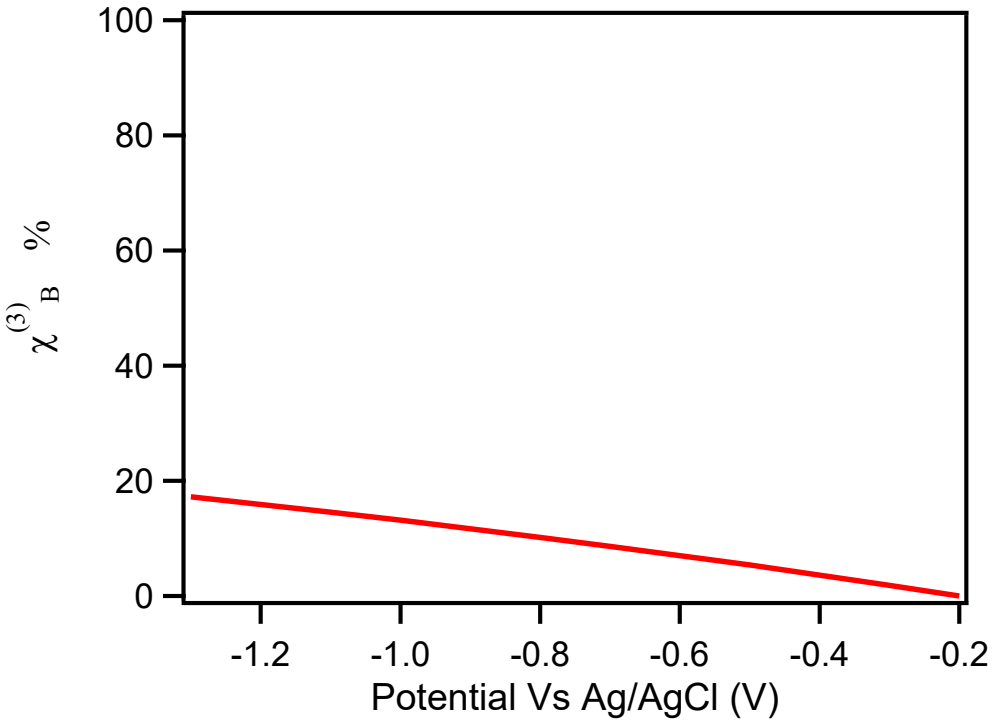

Figure S8. Estimated $\chi_B^{(3)}$ bulk contribution as a function of applied potential

Secondly, as pointed out by the reviewer and as shown in a previous study by Ohno et al [15], the contribution from $\chi_B^{(3)}$ for hydrogen bounded OH stretch signal can interfere with the 'free' OH stretch, and change the line shape of the free OH peak significantly. If the $\chi_B^{(3)}$ bulk signal is significant, we would see a line shape change of the free OH peak as more negative potentials are applied. Because at high potentials the $\chi_B^{(3)}$ bulk signal would increase significantly according to $\chi_{eff}^{(2)} = \chi_s^{(2)} + \chi_B^{(3)}\Phi$. On the contrary, the line shape of the free OH stretch shown in Figure 1a, Figure 2a, and Figure 4a did not change much as the potential changes from -0.2 V to -1.2 V. To compare the line shape of the free OH directly, the spectra of CO_2-saturated Na_2SO_4 solution at -0.2, -0.8, and -1.2 V are displayed together in the following figure.

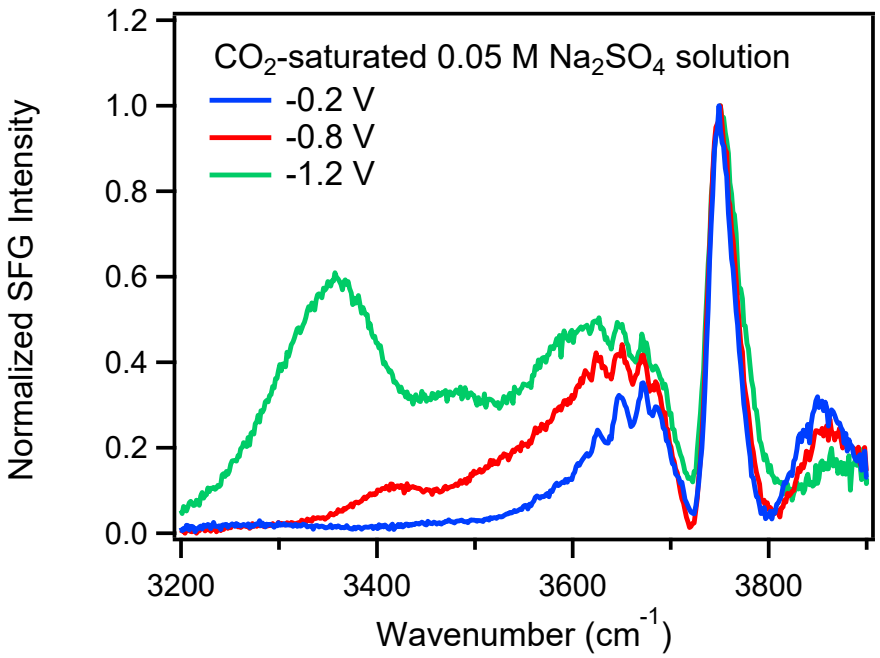

Figure S9. Normalized VSFG spectra of CO_2-saturated Na_2SO_4 solution at -0.2, -0.8, and -1.2 V.

To compare the line shape of the free OH directly, the peak intensity of the free OH are normalized to 1. It can be seen from Figure S9 that the line shape of the free OH remains almost unchanged when the potential changes from -0.2 V to -1.2 V. This further indicates that the $\chi_B^{(3)}$ bulk contribution in this work is not significant.

Lastly, as pointed out by several previous studies that the $\chi_B^{(3)}$ bulk contribution to the VSFG spectra resembles that of bulk water which has two major peaks around 3200 and 3450 cm^{-1} [8, 14, 15]. If there is significant $\chi_B^{(3)}$ bulk contribution in our spectra, we would see very pronounced peaks around 3200 cm^{-1} as shown by previous works. But the spectra in Figure 1a, Figure 2a, and Figure 4a for all three electrolyte solutions at all potentials show no apparent peak around 3200 cm^{-1}. For the Ar-saturated Na_2SO_4 solution, the whole H-bonded OH stretch region is almost flat. Based on this it appears that the $\chi_B^{(3)}$ bulk contribution is nearly negligible for the Ar-saturated Na_2SO_4 solution. For CO_2-saturated Na_2SO_4 and the Ar-saturated $NaHCO_3$ solutions, there are several peaks in the H-bonded OH stretch region. Two spectra of CO_2-saturated Na_2SO_4 and Ar-saturated $NaHCO_3$ solutions at -1.2 V are displayed together in the following figure.

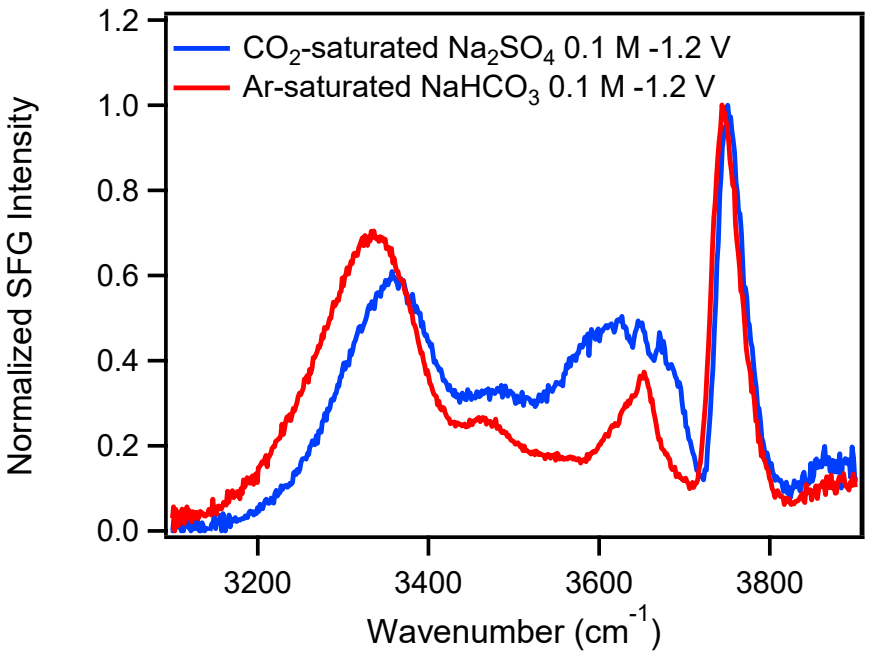

Figure S10. Normalized VSFG spectra of CO_2-saturated Na_2SO_4 and Ar-saturated $NaHCO_3$ solutions at -1.2 V.

It is shown in Figure S10 that there is small signal intensity around 3200 cm^{-1}, but no apparent peaks. The absence of the peak around 3200 cm^{-1} for all the spectra in this work further suggests that $\chi_B^{(3)}$ bulk contribution in the current work is not significant. Based on the above evidence it is safe to say that $\chi_B^{(3)}$ bulk contribution in our work is negligible and thus shouldn't affect our discussion.

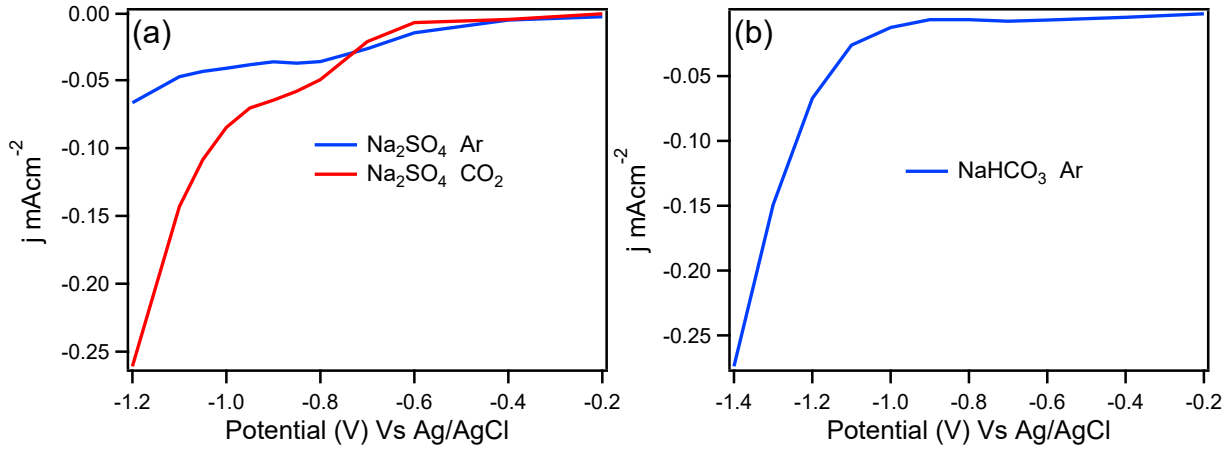

Figure S11. Current densities of Ar-, CO_2-saturated Na_2SO_4 and Ar-saturated $NaHCO_3$ solutions during SFG measurements.

6. LSV curve vs RHE

The onset potential change of HER is different for solutions with different pH. The pH of Ar and CO_2-saturated Na_2SO_4 solution are 7 and 5.6 respectively. Converting the potential to RHE can eliminate the influence of pH difference. Given $E_{(RHE)} = E_{Ag/AgCl} + 0.059\ pH + E^o_{Ag/AgCl}$, where $E^o_{Ag/AgCl}$=0.1976 V at 25°C, potential vs Ag/AgCl can be converted to $E_{(RHE)}$. Figure 3a is replotted Vs RHE as shown in Figure S11. The potential difference due to pH is only 0.08 V vs RHE as shown in Figure S11. Even on the RHE scale, the onset potential of the CO_2-saturated Na_2SO_4 solution is around -0.1 V which is about 0.1 V earlier than the Ar-saturated Na_2SO_4 solution. The current density of the CO_2-saturated Na_2SO_4 solution around -0.5 V is several times higher than that of the Ar-saturated Na_2SO_4 solution. Apparently, the onset potential change shown in Figure 3a cannot be explained solely by pH difference.

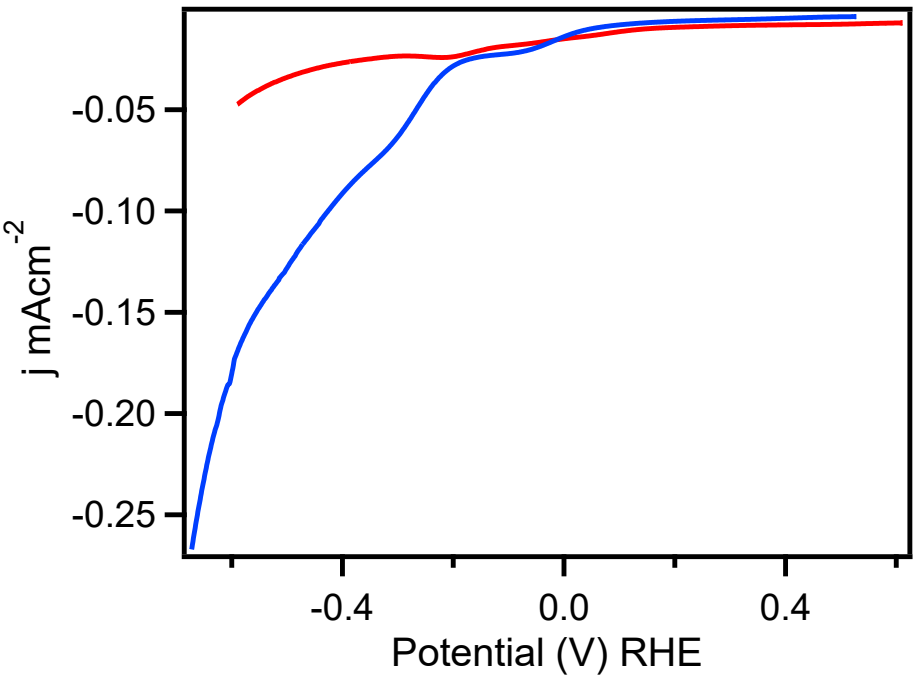

Figure S12. Linear sweep voltammograms. The current is normalized to the geometric area. The potential is converted to RHE.

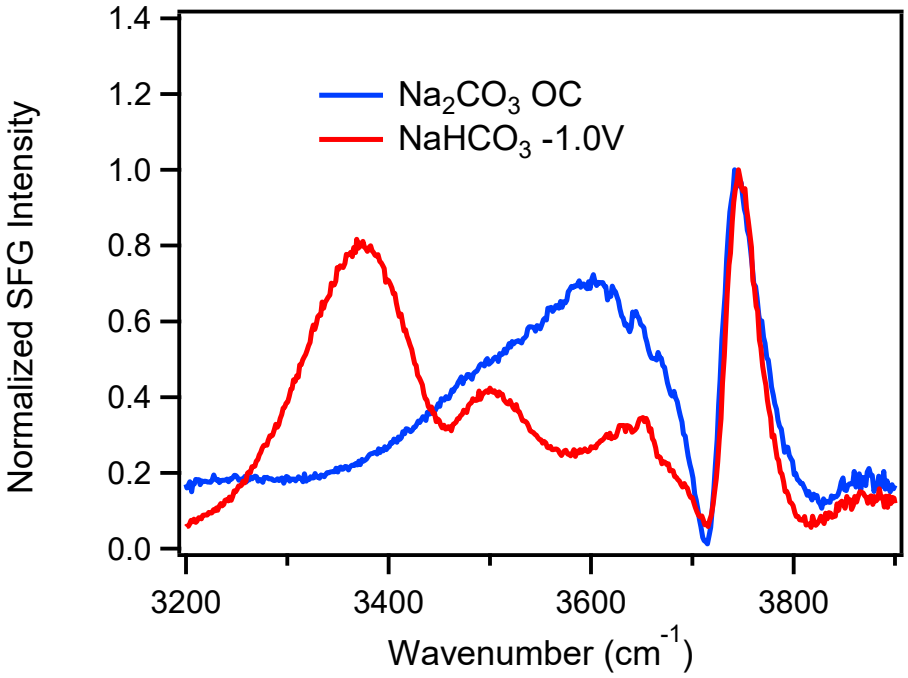

Figure S13. Normalized VSFG spectra of 0.1 M Na_2CO_3 at open circuit and Ar-saturated $NaHCO_3$ solutions at -1.0 V.

7. Fitting results of spectra in Figure 1a and Figure 4a

Table S1 The fitting parameters of the spectra in (Figure 1a) at Na_2SO_4 solution (0.05M)/gold interface for potentials from -0.8V— -1.1V. The spectra are fitted individually with the Lorentzian line shape function. The fitting parameters included the spectral amplitudes A_q, the resonant vibrational frequency ω_q and the peak width Γ_q.

Potential		3730	3650
-0.8V	A_q	1.9 ± 1.0	0.54 ± 0.84
	ω_q	3722.8±1.1	3654.4 ± 3.5
	Γ_q	26.6± 1.3	22.3 ± 3.1
-0.85V	A_q	2.2 ± 0.7	1.0 ± 0.3
	ω_q	3722.5± 0.8	3651.5 ± 1.0
	Γ_q	24.7± 0.9	16.4 ± 0.9
-0.9V	A_q	2.3 ± 0.5	1.4 ± 0.3
	ω_q	3722.0 ± 0.8	3651.2 ± 0.9
	Γ_q	24.1 ± 0.9	17.4 ± 0.8
-0.95V	A_q	2.6 ± 0.3	2.0 ± 0.2
	ω_q	3723.3 ± 0.6	3652.4 ± 0.5
	Γ_q	23.7 ± 0.7	16.2 ± 0.5
-1.0V	A_q	3.3 ± 0.2	3.2 ± 0.2
	ω_q	3724.1 ± 0.6	3653.3 ± 0.3
	Γ_q	23.9 ± 0.7	16.4 ± 0.3
-1.05V	A_q	3.6 ± 0.2	4.4 ± 0.2
	ω_q	3724.3 ± 0.6	3653.8 ± 0.3
	Γ_q	23.2 ± 0.7	17.0 ± 0.3
-1.1V	A_q	3.5 ± 0.2	4.9 ± 0.1
	ω_q	3725.4 ± 0.5	3653.9 ± 0.2
	Γ_q	22.1 ± 0.6	16.7 ± 0.2

Table S2 The fitting parameters of the spectra in (Figure 4a) at $NaHCO_3$ solution (0.1M)/gold interface for potentials from -0.8V— -1.4V. The spectra are fitted individually with the Lorentzian line shape function. The fitting parameters included the spectral amplitudes A_q, the resonant vibrational frequency ω_q and the peak width Γ_q.

Potential		3740	3650	3630	3600	3500	3400
-0.8V	A_q	7.1 ± 1.0	0.22 ± 1.2	121.3 ± 65.8		36.7 ± 12.6	17.8 ± 3.6
	ω_q	3739.8 ± 0.3	3653.2 ± 9.1	3645 ± 4.44		3538.2 ± 2.1	3437.9 ± 3.2
	Γ_q	15.4± 0.3	24.4 ± 49.7	122.8 ± 26.9		80.5 ± 7.0	61.3 ± 3.6
-0.9V	A_q	8.3 ± 0.3	0.46 ± 0.66	70.9 ± 9.9		28.9 ± 3.8	30.3 ± 1.3
	ω_q	3740.4 ± 0.3	3654.3 ± 3.5	3639.6 ± 3.1		3522.9 ± 1.1	3414.6 ± 1.3
	Γ_q	16.8 ± 0.3	20.0 ± 14.6	107.9 ± 9.1		66.8 ± 3.5	59.7 ± 1.2
-1.0V	A_q	8.5 ± 0.2	0.56 ± 0.73	70.6 ± 8.3		25.5 ± 3.1	39.0 ± 1.2
	ω_q	3740.1 ± 0.3	3651.8 ± 3.3	3636.8 ± 2.8		3512.1 ± 1.0	3398.1 ± 1.3
	Γ_q	17.6 ± 0.2	24.1 ± 14.8	113.4 ± 8.1		68.9 ± 3.3	71.2 ± 1.1
-1.1V	A_q	8.2 ± 0.3	1.23 ± 0.52	85.1 ± 11		26.2 ± 3.3	38.5 ± 1.3
	ω_q	3739.9 ± 0.2	3648.5 ± 1.1	3633.3 ± 2.6		3497.6 ± 1.0	3381.6 ± 1.3
	Γ_q	18.6 ± 0.2	25.4 ± 5.0	133.4 ± 9.4		79.17 ± 3.75	75.552 ± 1.1
-1.2V	A_q	9.0 ± 0.1	2.86 ± 0.1	56.3 ± 1.0		17.7 ± 0.8	37.9 ± 0.7
	ω_q	3740.6 ± 0.3	3649.3 ± 1.0	3622.4 ± 1.7		3483 ± 1.3	3357.6 ± 0.3
	Γ_q	19.6 ± 0.3	26.5 ± 1.5	134.7 ± 7.8		81.1 ± 4.6	81.2 ± 0.8
-1.3V	A_q	10.4 ± 0.2	6.5 ± 0.9	3.27 ± 1.13	4.0 ± 0.8	6.9 ± 1.2	32.4 ± 0.8
	ω_q	3741.7 ± 0.3	3653 ± 1.0	3617.1 ± 3.05	3548.2 ± 1.7	3467 ± 2.43	3328.3 ± 1.0
	Γ_q	22.2 ± 0.3	27.8 ± 1.6	32.1 ± 5.9	38.5 ± 4.9	61.5 ± 5.92	79.5 ± 1.4
-1.4V	A_q	10.4 ± 0.2	8.2 ± 0.4	1.4 ± 0.3	3.4 ± 0.3	5.0 ± 1.0	30.9 ± 0.7
	ω_q	3738.6 ± 0.3	3652.8 ± 0.5	3616.3 ± 1.4	3542.7 ± 0.8	3454.2 ± 2.5	3311.9 ± 1.1
	Γ_q	24.0 ± 0.3	28.4 ± 0.9	20.7 ± 2.7	28.9 ± 1.9	66.2 ± 7.8	78.5 ± 1.3

Reference

1. S. Wallentine, S. Bandaranayake, S. Biswas and L. R. Baker, *J. Phys. Chem. C*, 2020, **124**, 8057-8064.
2. S. Wallentine, S. Bandaranayake, S. Biswas and L. R. Baker, *J. Phys. Chem. Lett.*, 2020, **11**, 8307-8313.
3. J. A. Rebstock, Q. Zhu and L. R. Baker, *Chem. Sci.*, 2022, **13**, 7634-7643.
4. Q. Zhu, S. K. Wallentine, G.-H. Deng, J. A. Rebstock and L. R. Baker, *JACS Au*, 2022, **2**, 472-482.
5. H. Shang, S. K. Wallentine, D. M. Hofmann, Q. Zhu, C. J. Murphy and L. R. Baker, *Chem. Sci.*, 2020, **11**, 12298-12306.
6. M. Sovago, R. K. Campen, G. W. Wurpel, M. Müller, H. J. Bakker and M. Bonn, *Phys. Rev. Lett.* , 2008, **100**, 173901.
7. M. Nagao, K. Watanabe and Y. Matsumoto, *J. Phys. Chem. C*, 2009, **113**, 11712-11719.
8. A. Montenegro, C. Dutta, M. Mammetkuliev, H. Shi, B. Hou, D. Bhattacharyya, B. Zhao, S. B. Cronin and A. V. Benderskii, *Nature*, 2021, **594**, 62-65.
9. S. Pullanchery, S. Kulik, B. Rehl, A. Hassanali and S. Roke, *Science*, 2021, **374**, 1366-1370.
10. D. A. Wolf-Gladrow, R. E. Zeebe, C. Klaas, A. Körtzinger and A. G. Dickson, *Mar. Chem.* , 2007, **106**, 287-300.
11. J. J. Middelburg, in *Marine Carbon Biogeochemistry : A Primer for Earth System Scientists*, ed. J. J. Middelburg, Springer International Publishing, Cham, 2019, DOI: 10.1007/978-3-030-10822-9_5, pp. 77-105.
12. J. W. Morse and F. T. Mackenzie, *Geochemistry of sedimentary carbonates*, Elsevier, 1990.
13. S. Ong, X. Zhao and K. B. Eisenthal, *Chem. Phys. Lett.* , 1992, **191**, 327-335.
14. Y.-C. Wen, S. Zha, X. Liu, S. Yang, P. Guo, G. Shi, H. Fang, Y. R. Shen and C. Tian, *Phys. Rev. Lett.* , 2016, **116**, 016101.
15. P. E. Ohno, H.-f. Wang and F. M. Geiger, *Nat. Commun.*, 2017, **8**, 1032.
16. P. E. Ohno, H.-f. Wang, F. Paesani, J. L. Skinner and F. M. Geiger, *J. Phys. Chem. C*, 2018, **122**, 4457-4464.
17. A. J. Lock, S. Woutersen and H. J. Bakker, *J. Phys. Chem. C*, 2001, **105**, 1238-1243.
18. A. Eftekhari-Bafrooei and E. Borguet, *J. Phys. Chem. Lett.*, 2011, **2**, 1353-1358.
19. S. Xiao, F. Figge, G. Stirnemann, D. Laage and J. A. McGuire, *J. Am. Chem. Soc.* , 2016, **138**, 5551-5560.